J Neurophysiol 94: 2105–2110, 2005.
First published June 15, 2005; doi:10.1152/jn.00414.2005.

Effects of Salicylate on Plasma Membrane Mechanics

Sergey A. Ermilov,[1] David R. Murdock,[1] Dania El-Daye,[1] William E. Brownell,[2] and Bahman Anvari[1]
[1]*Department of Bioengineering, Rice University; and* [2]*Department of Otorhinolaryngology and Communicative Sciences, Baylor College of Medicine, Houston, Texas*

Submitted 22 April 2005; accepted in final form 7 June 2005

Ermilov, Sergey A., David R. Murdock, Dania El-Daye, William E. Brownell, and Bahman Anvari. Effects of salicylate on plasma membrane mechanics. *J Neurophysiol* 94: 2105–2110, 2005. First published June 15, 2005; doi:10.1152/jn.00414.2005. High concentrations of the amphipathic drug salicylate (Sal) block outer hair cell (OHC) electromotility resulting in reversible hearing loss. We used optical tweezers to study the effects of Sal on the mechanics of the cell plasma membrane. Membrane tethers were formed from guinea pig OHCs and cultured human embryonic kidney (HEK) cells as controls. HEK cells are commonly used in functional expression studies of electromotility. Effective tether viscosity (η_{eff}), steady-state tethering force extrapolated to zero pulling rate $F_{ss(0)}$, and time constant for tether growth (τ_{tg}) were estimated from the measurements of the instantaneous tethering force at different tether pulling rates. Average values of η_{eff}, $F_{ss(0)}$, and τ_{tg} for the OHC lateral wall plasma membrane and control cell plasma membrane remained the same after Sal perfusion, which is consistent with the hypothesis that Sal-induced reversible hearing loss appears to be more the result of its competition with essential anions and less the result of a change in plasma membrane mechanics.

INTRODUCTION

Cochlear outer hair cells (OHCs) are specialized sensory/motor cells capable of producing electrically evoked length changes (Brownell 1984; Brownell et al. 1985). The force responsible for this electromotility provides additional mechanical energy to the vibrating structures of the inner ear and functions to narrow the band-pass filtering at a given location along the length of the cochlear partition (Brownell et al. 1985, 2001; Dallos and Corey 1991). Electrically induced forces are generated within the plasma membrane (PM) of the OHC lateral wall. The transmembrane OHC protein, prestin, has been shown to endow rudimentary electromotility in transfected cells (Zheng et al. 2000). The manner by which prestin enhances the piezoelectric-like membrane behavior (Brownell 2005; Dong et al. 2002; Ludwig et al. 2001; Qian et al. 2004) is not clear; however, it must interact with the membrane in which it resides to function. The PM interacts with an underlying cytoskeletal cortical lattice (CL) through radially oriented pillars, which are thought to transfer the forces generated in the PM to the CL. The pillars have an unknown molecular composition. The CL is organized into microdomains composed of parallel F-actin filaments that on average run circumferentially. The actin filaments are crosslinked with spectrin (Brownell et al. 2001; Holley et al. 1992).

Prestin-transfected human embryonic kidney (HEK) cells have been used in functional expression studies of electromotility (Ludwig et al. 2001; Zheng et al. 2000). HEK cells have a morphology different from that of cylindrically shaped OHCs, lack the orthotropically organized CL of OHCs, and do not have pillars linking the PM to the cytoskeleton.

Electromotility involves a coupling of electrical and mechanical properties of the membrane, which is the rationale for characterizing the mechanics of the membrane. Models of membrane-based electromotility (Brownell et al. 2001; Petrov and Sachs 2002; Raphael et al. 2000) depend on both mechanical and electrical properties of the PM. Therefore chemical agents, which can alter mechanical or electrical characteristics of PM, may also affect electromotility. Amphipaths are agents that are both water and lipid soluble. Salicylate (Sal), the anionic amphipathic metabolite of aspirin, has long been known to increase the local outward bending of the red blood cell PM (Sheetz and Singer 1976). Early experiments suggested that it introduces additional negative surface charge (McLaughlin 1973). Sal reversibly induces hearing loss and suppresses electromotility of OHCs (Dieler et al. 1991; Kakehata and Santos-Sacchi 1996; Shehata et al. 1991) and prestin-transfected HEK cells (Zheng et al. 2000). There are two studies that report an effect of Sal on electromotility without changes in the measured cellular mechanical parameters: *1*) Hallworth (1997) demonstrated a reduction in electrically evoked force production without an effect on OHC axial stiffness; *2*) Zhang et al. (2001) used atomic force microscopy on wild-type HEK cells and found that Sal produced no change in membrane indentation profiles (force-displacement functions in the absence of electrical stimulation) but did reduce electromotility. Sal may also compete with intracellular Cl^- ions, which have been found essential for OHC electromotility (Oliver et al. 2001). There is also a Sal-induced reduction in lipid lateral diffusion in the OHC lateral wall PM (Oghalai et al. 2000).

Single-beam gradient force optical traps (optical tweezers) can be used to form and stretch a thin strand (tether) of PM using a trapped microsphere as a "handle." The tether is a long ($\leq$100 μm) cylinder of membrane with a diameter of $<$100 nm. Displacement of the trapped microsphere is used to measure membrane-generated forces, allowing estimates of some PM mechanical properties (Li et al. 2002; Raucher and Sheetz 1999). In this work we use optical tweezers to characterize mechanical properties of the OHC and HEK cell PM with and without extracellular perfusion of 10 mM sodium Sal. We pull PM tethers and analyze the temporal tethering force profiles to quantify parameters related to mechanical characteristics of the PM.

Address for reprint requests and other correspondence: B. Anvari, Rice University, Department of Bioengineering, P.O. Box 1892, MS 142, Houston, TX 77251-1892 (E-mail: anvari@rice.edu).

The costs of publication of this article were defrayed in part by the payment of page charges. The article must therefore be hereby marked "*advertisement*" in accordance with 18 U.S.C. Section 1734 solely to indicate this fact.

METHODS

Experimental setup and trapping force calibration

The optical tweezers setup and trapping force calibration technique are fully described in our previous works (Qian et al. 2004). In brief, we used a continuous wave titanium–sapphire laser beam tuned to 830 nm, passed through a high numerical aperture (NA = 1.3) oil immersion microscope objective, to form an optical trap. A position-sensing quadrant photodetector (QPD) was used to measure the transverse displacement of a trapped 4-μm-diameter sulfate-modified fluorescent polystyrene microsphere (F-8858, Molecular Probes, Eugene, OR) from the trapping center in response to the force generated by stretching the PM tether. To calibrate the QPD output voltage versus trapping force a piezostage (PZT) was used to induce a viscous drag force against the trapped microsphere by moving the fluid-filled sample chamber. The PZT was operated with control electrical signals consisting of triangular waveforms, 5-V peak-to-peak amplitude, and frequencies in the range from 1 to 6 Hz, where amplitude response of the trapping force is close to 1 (Ermilov and Anvari 2004). Calibration was performed before every experiment.

Preparing OHCs and HEK cells

Pigmented guinea pigs of either sex weighing 200–250 g were decapitated following an institutionally approved protocol at the Baylor College of Medicine (protocol AN1105). Both cochlea were dissected from temporal bones, and placed into the 10 mM sodium salicylate (NaSal) solution containing (in mM): 132 NaCl, 5.37 KCl, 1.47 $MgCl_2$, 2 $CaCl_2{\cdot}2H_2O$, 10 NaSal, and 10 HEPES. This particular concentration of Sal was used because in OHCs it induces maximum reduction of the peak nonlinear capacitance, associated with electromotility (Kakehata and Santos-Sacchi 1996). For control experiments we used normal extracellular solution (NES) containing (in mM): 142 NaCl, 5.37 KCl, 1.47 $MgCl_2$, 2 $CaCl_2{\cdot}2H_2O$, and 10 HEPES. The pH of both Sal and NES solutions was adjusted to 7.2–7.4 using 1 M NaOH. The Sal and NES osmolarity was adjusted with D-glucose to 300 ± 5 mOsm. Each cochlea was carefully opened by a scalpel, and organ of Corti was transferred into the NES solution containing 0.5 mg/ml trypsin. After 5 min of incubation most of the OHCs were dispersed from the supporting cells, and harvested using a microsyringe to a poly-D-lysine–coated sample chamber with 1.5 ml of pure NES or Sal. OHCs were allowed to adhere to the bottom of a sample chamber for 10 min. Microspheres were then added to the bathing solution. A medium-size OHC (population distribution: 55–85 μm long and 8–10 μm in diameter) was selected for measurements if it exhibited a cylindrical shape with a basally located nucleus, with limited osmotic swelling and no cytoplasmic particles exhibiting Brownian motion. All OHCs were used within 4 h after the animal was decapitated.

Cultured HEK-293 cells (Advanced Cell Technology, Worcester, MA) were passaged into the sample chamber and left in an incubator for 2 h. After the cells adhered to the bottom of the sample chamber, the culture medium was substituted with 1.5 ml of an extracellular solution and microspheres were added. A medium-size (population distribution: 10–20 μm in diameter) HEK cell was selected for measurements if it had rounded shape and the cytoplasm was agranular. All experiments on HEK cells were performed within 2 h of removal from the incubator.

Coating microspheres

Previous HEK experiments using fluorescent microspheres required coating the sample chamber with an antimycotic solution to prevent undesired bead adhesion (Ermilov et al., unpublished observations). OHCs were found to deteriorate quickly under these conditions. Therefore we decided to coat fluorescent microspheres with bovine serum albumin (BSA). We incubated 50 μl of fluorescent microspheres with 1 ml of 10 mg/ml aqueous BSA (Fisher Scientific, Hampton, NH) solution overnight under gentle mixing. The success rate of a microsphere detachment from the coverslip of a sample chamber using optical tweezers increased from 0 to >10% after microspheres were coated with BSA.

Experimental procedure

During experiments, an OHC or HEK cell, firmly attached to the coverslip, was identified by microscopic scanning through the sample chamber. Then, a microsphere, floating nearby the cell, was optically trapped. Microscope stage manipulators were used to move the cell toward the microsphere until they were in physical contact. We allowed the microsphere to adhere to the cell PM for 5 s and then triggered a synthesized function generator, which generated a waveform function to control the PZT movement such that the cell was moved away from the trapped microsphere at 1 μm/s speed for 10 s. During this time a PM tether was usually formed. Speed of the PZT was subsequently increased every 2 s by 1 μm/s until it reached 6 μm/s.

Data analysis

Tether formation involves separation of the membrane from the cytoskeleton. The tether growth process is the subsequent elongation of the tether, which is reflected in the temporal force profile. We analyzed temporal tethering force profiles (Fig. 1*A*) to obtain the parameters related to the viscoelastic behavior of the PM tether. We observed that when a tether was pulled at a constant velocity, the tethering force reached a steady-state value, F_{ss}, which remained approximately constant with increasing tether length. The last 100 values of the tethering force signal recorded for 1 μm/s pulling rate were averaged to estimate the steady-state tethering force at 1 μm/s pulling rate. Each individual part of a tethering force signal recorded for the i-th pulling segment at a specific pulling rate, starting with 2 μm/s, was fit with an exponential function (Fig. 1*B*) with unknown change in steady-state tethering force [$\Delta F_{ss(i)}$], and the time constant for tether growth [$\tau_{tg(i)}$]

$$F_{teth(i)}(t) = F_{teth(i-1)end} + \Delta F_{ss(i)} \cdot \left\{1 - \exp\left[-\frac{t - t_{(i-1)end}}{\tau_{tg(i)}}\right]\right\} \quad i = 2, 3, \ldots, 6 \tag{1}$$

where t is the time elapsed from the beginning of pulling; $F_{teth(i)}(t)$ is the tethering force measured at time t for the i-th pulling segment; $F_{teth(i-1)end}$ is the last value of the tethering force measured for the (i − 1)-th pulling segment; and $t_{(i-1)end}$ is the time corresponding to the last value of the tethering force measured for the (i − 1)-th pulling segment. The exponential increase of the tethering force after a sudden increase in the tether pulling rate was first reported in our previous publication (Li et al. 2002).

Using the obtained values of $\Delta F_{ss(i)}$, we calculated the steady-state tethering forces as

$$F_{ss(i)} = F_{teth(i-1)end} + \Delta F_{ss(i)} \tag{2}$$

where $F_{ss(i)}$ is the asymptotic value of the steady-state tethering force calculated for the i-th pulling segment (i = 2, 3, . . . , 6).

The calculated data for the steady-state tethering forces at each tether pulling rate (V_{pull}) were fit (Fig. 2) with a linear function (Hochmuth et al. 1996) to estimate the unknown steady-state tethering force extrapolated to the zero pulling rate $F_{ss(0)}$ and effective tether viscosity (η_{eff})

$$F_{ss}(V_{pull}) = F_{ss(0)} + 2\pi\eta_{eff}V_{pull} \tag{3}$$

Values of $F_{ss(0)}$, η_{eff}, and τ_{tg} averaged over all pulling segments were used in our studies to compare the viscoelastic properties of the

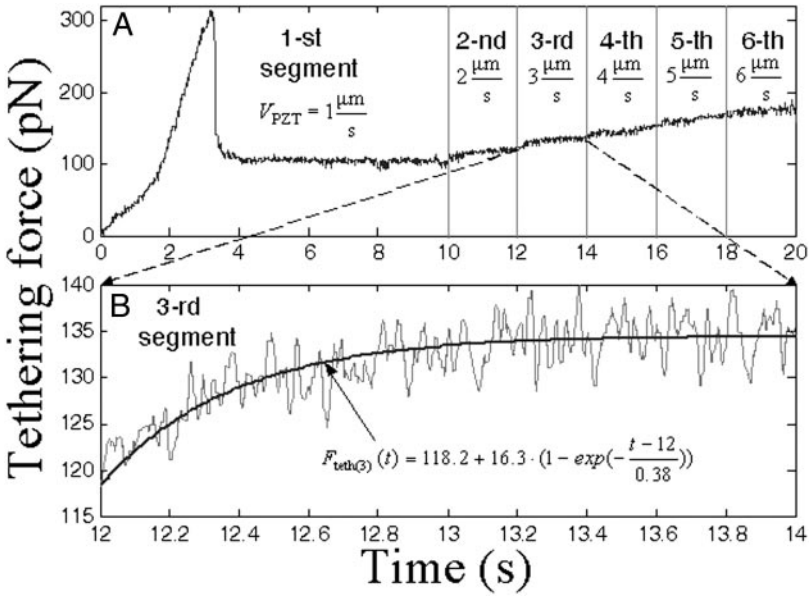

FIG. 1. *A*: typical temporal tethering force profile measured at increasing pulling rates. *B*: enlarged view of the 3-rd segment from the temporal tethering force profile shown in *A*, and its fit with the exponential function (*Eq. 1*): $F_{teth(2)end} = 118.2$ pN, $\Delta F_{ss(3)} = 16.3$ pN, $t_{(2)end} = 12$ s, $\tau_{tg(3)} = 0.38$ s.

PM for different cells and experimental conditions. Statistical analysis of the differences in the mean values of calculated parameters was performed on OHCs and HEK cells, and on cells of the same type perfused with NES and Sal solution. We used unpaired *t*-test, assuming normal populations with unknown variances, and statistical significance was accepted if the *P* value was <0.05.

RESULTS

Steady-state tethering force extrapolated to zero pulling rate

Average steady-state tethering forces extrapolated to zero pulling rate (±SD) for OHC lateral wall, OHC basal end, and HEK cells, perfused with NES, were 103.4 ± 28.4 ($N = 17$), 81.5 ± 22.9 ($N = 11$), and 43.1 ± 13.6 ($N = 15$) pN, respectively (Fig. 3). The presence of NaSal resulted in $F_{ss(0)}$ mean values of 99.2 ± 25.6 ($N = 13$), 79.7 ± 29 ($N = 14$), and 42.3 ± 9.9 ($N = 7$) pN for OHC lateral wall, OHC basal end, and HEK cells, respectively (Fig. 3). The differences between the mean values of $F_{ss(0)}$ for the cells perfused with NES were statistically different for OHC lateral wall and basal end ($P = 0.034$), OHC lateral wall and HEK cells ($P < 0.001$), and OHC basal end and HEK cells ($P < 0.001$). No statistically significant differences in the mean values of $F_{ss(0)}$ were found between the cells perfused with NES and 10 mM NaSal (Fig. 3).

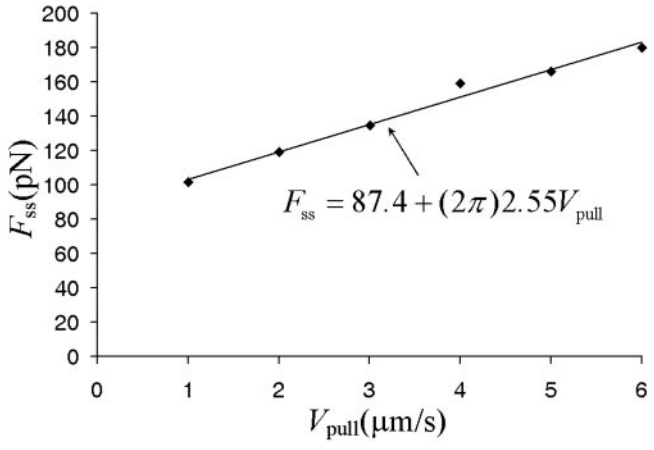

FIG. 2. Plot of steady-state tethering forces vs. tether pulling rates. $F_{ss(0)}$ and η_{eff} were calculated from a linear fit (*Eq. 3*) to the data points: $r^2 = 0.9835$, $F_{ss(0)} = 87.4$ pN, $\eta_{eff} = 2.55$ pN/(μm/s). Steady-state forces were calculated from data shown in Fig. 1*A*, using *Eq. 1*.

Effective tether viscosity

Average effective tether viscosities (±SD) for OHC lateral wall, OHC basal end, and HEK cells, perfused with NES, were 1.70 ± 0.58 ($N = 17$), 1.71 ± 0.64 ($N = 11$), and 1.39 ± 0.56 ($N = 15$) pN/(μm/s), respectively (Fig. 4). The presence of NaSal resulted in η_{eff} mean values of 1.69 ± 0.62 ($N = 13$), 1.65 ± 0.78 ($N = 14$), and 1.31 ± 0.34 ($N = 7$) pN/(μm/s) for OHC lateral wall, OHC basal end, and HEK cells, respectively (Fig. 4). No statistically significant differences in the mean values of η_{eff} were found between OHCs and HEK cells, and between cells perfused with NES and 10 mM NaSal (Fig. 4).

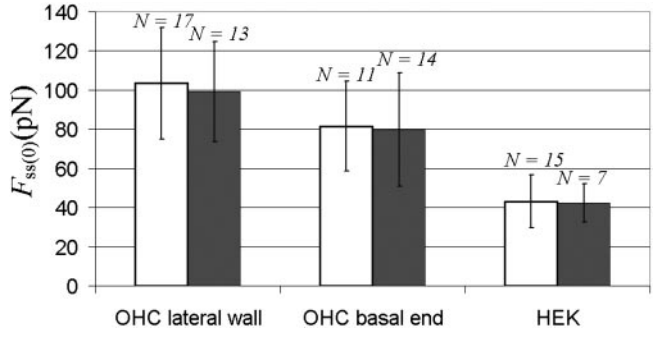

FIG. 3. Steady-state tethering force extrapolated to zero tether pulling rate, $F_{ss(0)}$ ± SD (pN). □: cells perfused with normal extracellular solution: outer hair cell (OHC) lateral wall 103.4 ± 28.4 ($N = 17$), OHC basal end 81.5 ± 22.9 ($N = 11$), human embryonic kidney (HEK) cells 43.1 ± 13.6 ($N = 15$); ■: cells perfused with 10 mM sodium salicylate (NaSal): OHC lateral wall 99.2 ± 25.6 ($N = 13$), OHC basal end 79.7 ± 29 ($N = 14$), HEK cells 42.3 ± 9.9 ($N = 7$). Mean values of $F_{ss(0)}$ for the basal end and HEK cell were both statistically different from that for the lateral wall; the HEK cell value was also statistically different from the basal end ($P < 0.05$ for all comparisons). Differences between the normal and Sal-treated membranes were not significant.

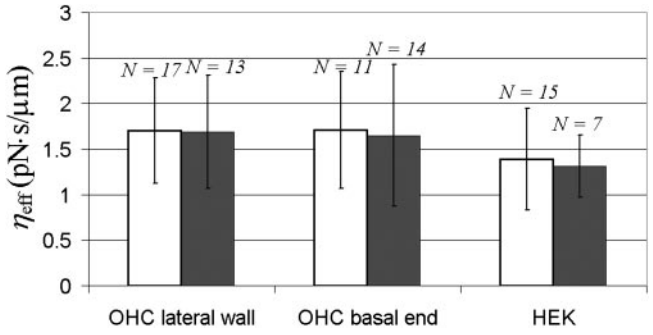

FIG. 4. Effective tether viscosity, $\eta_{eff} \pm$ SD [pN/(μm/s)]. □: cells perfused with normal extracellular solution: OHC lateral wall 1.70 ± 0.58 (N = 17), OHC basal end 1.71 ± 0.64 (N = 11), HEK cells 1.39 ± 0.56 (N = 15); ■: cells perfused with 10 mM NaSal: OHC lateral wall 1.69 ± 0.62 (N = 13), OHC basal end 1.65 ± 0.78 (N = 14), HEK cells 1.31 ± 0.34 (N = 7). Differences between the normal and Sal-treated membranes and between the different groups were not significant.

Time constant for the tether growth

Average time constants for tether growth (± SD) for OHC lateral wall, OHC basal end, and HEK cells, perfused with NES, were 0.92 ± 0.44 (N = 18), 1.51 ± 0.60 (N = 14), and 1.07 ± 0.52 (N = 15) s, respectively (Fig. 5). The presence of NaSal resulted in τ_{tg} mean values of 1.08 ± 0.82 (N = 15), 0.94 ± 0.46 (N = 16), and 0.99 ± 0.42 (N = 7) s for OHC lateral wall, OHC basal end, and HEK cells, respectively (Fig. 5). The mean values of τ_{tg} for the cells perfused with NES were statistically different between OHC lateral wall and basal end (P = 0.005) and OHC basal end and HEK cells (P = 0.046). There was no significant difference for the OHC lateral wall PM and HEK cell PM as well as for the OHC lateral wall and HEK PM in the absence and the presence of Sal. A statistically significant difference (P = 0.008) was found for the mean values of τ_{tg} in OHC basal end between cells perfused with NES and 10 mM NaSal.

DISCUSSION

The PM tether is a structure held at equilibrium between photonic forces acting on the trapped bead and those forces resulting from the effective cell membrane tension. The effective cell membrane tension refers to the mechanical tension generated in the PM by the combination of osmotic conditions, PM–cytoskeleton interaction at discrete PM confinement sites (Fournier et al. 2004; Gov et al. 2003, 2004) and local and nonlocal PM curvature elasticity (Hochmuth et al. 1996; Waugh et al. 1992).

The parameter $F_{ss(0)}$ is the force required to hold a PM tether at static equilibrium. It is extrapolated from the steady-state tethering forces measured at known tether pulling rates. Our values of $F_{ss(0)}$ for outer hair cells are in the range reported by Li et al. (2002) for static tether forces, which were measured with optically trapped microspheres using a different protocol.

OHCs are cellular hydrostats (Brownell 2005), making them sensitive to changes in the osmolarity of the bathing media. We were careful to maintain extracellular osmolarity at the same value and any change in the bathing osmolarity during the experiment would be immediately obvious by changes in cell length. Therefore the major contribution to the differences in $F_{ss(0)}$ among OHCs and HEK cells comes from cell-specific internal osmotic conditions, PM–cytoskeleton interactions, and/or bending properties of the PM.

Cholesterol may increase PM bending resistance, and consequently the $F_{ss(0)}$ value, by increasing the lipid bilayer rigidity. There is evidence suggesting membrane cholesterol is at a higher concentration in the OHC basal end than that in the OHC lateral wall (Nguyen and Brownell 1998). The nearly 90% greater $F_{ss(0)}$ for the OHC basal end compared with that of HEK cells might be explained by a greater cholesterol concentration in the OHC basal membrane than that in the HEK PM. However, the $F_{ss(0)}$ for the lateral wall PM is 27% greater than the $F_{ss(0)}$ for basal PM. Therefore factors other than cholesterol concentration must contribute to the $F_{ss(0)}$ in the lateral wall PM. These may include large amounts of PM-associated proteins not found in the OHC basal end, including prestin, glucose transporters, as well as the pillars.

The nonzero value of η_{eff} implies the existence of viscous-like dissipation during tether pulling. In our studies we found η_{eff} to be on the order of 1.3–1.7 pN/(μm/s) with no statistically significant differences among the OHC lateral wall, OHC basal end, and HEK cells. The values are about half of those reported by Li et al. (2002). We attribute this fact to possible differences in the procedures of microsphere attachment to the plasma membrane. In this work using fluorescent microspheres we were able to control the initiation of microsphere–plasma membrane physical contact by observing the force deviation from an initial zero value rather than just attempting to visually estimate the contact. Our values of η_{eff} are also two orders of magnitude greater than the reported η_{eff} for pure phospholipid vesicles (Evans and Yeung 1994; Waugh 1982), which supports the hypothesis (Hochmuth et al. 1996; Li et al. 2002) that in cells η_{eff} is dominated by interactions between the PM and underlying cytoskeleton.

The parameter τ_{tg} indicates how fast the tethering force approaches its steady-state value after a sudden increase in the pulling rate. The greater the value of τ_{tg}, the slower the tethering force will be increasing. It is related to the viscoelastic properties of the PM, mass of the trapped microsphere, viscosity of the extracellular solution, and transverse stiffness of the optical trap. Smaller effective cell membrane tension or larger η_{eff} increases the τ_{tg} value, similar to the way it happens

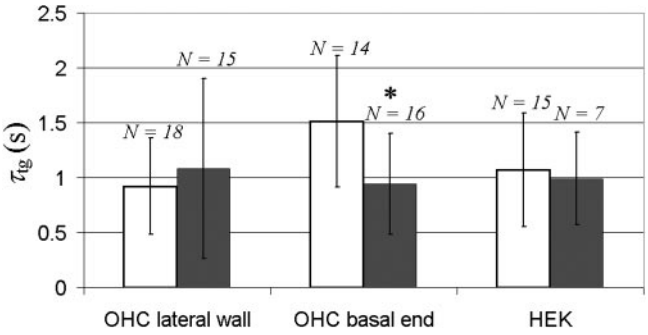

FIG. 5. Average time constant for the tether growth, $\tau_{tg} \pm$ SD (s). □: cells perfused with normal extracellular solution: OHC lateral wall 0.92 ± 0.44 (N = 18), OHC basal end 1.51 ± 0.60 (N = 14), HEK cells 1.07 ± 0.52 (N = 15); ■: cells perfused with 10 mM NaSal: OHC lateral wall 1.08 ± 0.82 (N = 15), OHC basal end 0.94 ± 0.46 (N = 16), HEK cells 0.99 ± 0.42 (N = 7). Mean value of τ_{tg} for the basal end was significantly larger than for the other non-Sal–treated cell groups. There was no significant difference between the Sal-treated groups. Difference between the normal and Sal-treated membranes within groups was not significant except for the basal end (*$P < 0.05$).

in a model composed of a dashpot and a spring connected in parallel. Therefore the smaller value of $F_{ss(0)}$ (directly related to the effective PM tension) for OHC basal end compared with that for the lateral wall would contribute to the observed increased value of τ_{tg} for the OHC basal end. On the other hand, the smaller value of η_{eff} for HEK cells compared to that for the OHCs could counteract the increase of τ_{tg} anticipated because of the smaller values of $F_{ss(0)}$.

The data show that addition of Sal does not cause significant changes in the calculated parameters (excluding τ_{tg} for the OHC basal end). Using a micropipette aspiration technique, Morimoto et al. (2002) showed no effect of Sal on PM vesiculation pressure, a parameter related to the strength of PM–cytoskeleton interaction. Our experiments showed that Sal does not affect η_{eff}, which is consistent with findings by Morimoto et al. (2002). The lack of changes in PM viscoelastic parameters after extracellular application of Sal is consistent with the studies of the voltage-induced movement on the PM of HEK cells as measured with an atomic force microscope cantilever (Zhang et al. 2001). Although Sal blocked electrically evoked PM movement, there was no statistically significant effect of Sal on the force–indentation depth curves. Force–indentation depth curves from the atomic force microscopy studies as well as the steady-state tethering force extrapolated to zero pulling rate are dependent on the effective cell membrane tension, and thus the similar observation of the lack of Sal effect on both mechanical characteristics strengthens the hypothesis that Sal does not change effective cell membrane tension. These results are compatible with those showing no effect of Sal on OHC axial compliance but reducing OHC electromotility (Hallworth 1997). In a separate study we have also shown that Sal reduces electrically evoked force generation in PM tethers from wild-type HEK cells (Anvari et al. 2005).

The absence of a change in membrane mechanics supports the concept that both OHC and HEK cell electromotility involve an interaction between Sal and the surface charge of the membrane. There is evidence that Sal anions compete with intracellular Cl^-, decreasing the availability of Cl^- required for electromotility (Oliver et al. 2001). Salicylate's phenol group is thought to partition into the hydrophobic phase of a plasma membrane whereas its hydroxyl group produces additional negative surface charge by partitioning into the phospholipids headgroup region (McLaughlin 1973; Song and Baker 2005). McLaughlin (1973) argued that the salicylate-induced change in surface charge contributes to decreased anion permeability and an increased cation permeability. A decreased membrane permeability for the Cl anions is of particular importance for OHCs because at a constant holding electrical potential it would lead to depletion of the intracellular chloride pool, with subsequent reduction of electromotility. These observations all suggest that Sal reduces electromotility by an electrochemical interaction involving chloride.

ACKNOWLEDGMENTS

We thank C. Shope for assistance with outer hair cells and human embryonic kidney cell cultures.

GRANTS

This work was supported in part by National Institute of Deafness and Other Communication Disorders Grant 2R01-DC-02775-06.

REFERENCES

Anvari B, Qian F, Pereria FA, and Brownell WE. Prestin-lacking membranes are capable of high frequency electro-mechanical transduction. In: *Auditory Mechanisms: Processes and Models*, edited by Nuttall AL. London: World Scientific, 2005.

Brownell WE. Microscopic observation of cochlear hair cell motility. *Scanning Electron Microsc* III: 1401–1406, 1984.

Brownell WE. The piezoelectric outer hair cell. In: *Handbook of Auditory Research*, edited by Popper AN and Fay RR. New York: Springer-Verlag, 2005, chap. 7.

Brownell WE, Bader CR, Bertrand D, and de Ribaupierre Y. Evoked mechanical responses of isolated cochlear outer hair cells. *Science* 227: 194–196, 1985.

Brownell WE, Spector AA, Raphael RM, and Popel AS. Micro- and nanomechanics of cochlear outer hair cell. *Annu Rev Biomed Eng* 3: 169–194, 2001.

Dallos P and Corey ME. The role of outer hair cell motility in cochlear tuning. *Curr Opin Neurobiol* 1: 215–220, 1991.

Dieler R, Shehata-Dieler WE, and Brownell WE. Concomitant salicylate-induced alterations of outer hair cell subsurface cisternae and electromotility. *J Neurocytol* 20: 637–653, 1991.

Dong XX, Ospeck M, and Iwasa KH. Piezoelectric reciprocal relationship of the membrane motor in the cochlear outer hair cell. *Biophys J* 82: 1254–1259, 2002.

Ermilov S and Anvari B. Dynamic measurements of transverse optical trapping force in biological applications. *Ann Biomed Eng* 32: 1017–1027, 2004.

Evans EA and Yeung A. Hidden dynamics in rapid changes of bilayer shape. *Chem Phys Lipids* 73: 39–56, 1994.

Fournier J-B, Lacoste D, and Raphael E. Fluctuation spectrum of fluid membranes coupled to an elastic meshwork: jump of the effective surface tension at the mesh size. *Phys Rev Lett* 92: 018102, 2004.

Gov N and Safran SA. Pinning of fluid membranes by periodic harmonic potentials. *Phys Rev E* 69: 011101, 2004.

Gov N, Zilman AG, and Safran S. Cytoskeleton confinement and tension of red blood cell membranes. *Phys Rev Lett* 90: 228101, 2003.

Hallworth R. Modulation of outer hair cell compliance and force by agents that affect hearing. *Hear Res* 114: 204–212, 1997.

Hochmuth RM, Shao J-Y, Dai J, and Sheetz MP. Deformation and flow of membrane into tethers extracted from neuronal growth cones. *Biophys J* 70: 358–369, 1996.

Holley MC, Kalinec F, and Kachar B. Structure of the cortical cytoskeleton in mammalian outer hair cells. *J Cell Sci* 102: 569–580, 1992.

Kakehata S and Santos-Sacchi J. Effects of salicylate and lanthanides on outer hair cell motility and associated gating charge. *J Neurosci* 16: 4881–4889, 1996.

Li Z, Anvari B, Takashima M, Brecht P, Torres JH, and Brownell WE. Membrane tether formation from outer hair cells with optical tweezers. *Biophys J* 82: 1386–1395, 2002.

Ludwig J, Oliver D, Frank G, Klocker N, Gummer AW, and Fakler B. Reciprocal electromechanical properties of rat prestin: the motor molecule from rat outer hair cells. *Proc Natl Acad Sci USA* 98: 4178–4183, 2001.

McLaughlin S. Salicylates and phospholipid bilayer membranes. *Nature* 243: 234–236, 1973.

Morimoto N, Raphael RM, Nygren A, and Brownell WE. Excess plasma membrane and effects of ionic amphipaths on mechanics of outer hair cell lateral wall. *Am J Physiol Cell Physiol* 282: C1076–C1086, 2002.

Nguyen TV and Brownell WE. Contribution of membrane cholesterol to outer hair cell lateral wall stiffness. *Otolaryngol Head Neck Surg* 119: 14–20, 1998.

Oghalai JS, Zhao H, Kutz JW, and Brownell WE. Voltage- and tension-dependent lipid mobility in the outer hair cell plasma membrane. *Science* 287: 658–661, 2000.

Oliver D, He DZZ, Klocker N, Ludwig J, Schulte U, Waldegger S, Ruppersberg JP, Dallos P, and Fakler B. Intracellular anions as the voltage sensor of prestin, the outer hair cell motor protein. *Science* 292: 2340–2343, 2001.

Petrov AG and Sachs F. Flexoelectricity and elasticity of asymmetric biomembranes. *Phys Rev E* 65: 021905, 2002.

Qian F, Ermilov S, Murdock D, Brownell WE, and Anvari B. Combining optical tweezers and patch clamp for studies of cell membrane electromechanics. *Rev Sci Instrum* 75: 2937–2942, 2004.

Raphael RM, Popel AS, and Brownell WE. A membrane bending model of outer hair cell electromotility. *Biophys J* 78: 2844–2862, 2000.

Raucher D and Sheetz MP. Characteristics of a membrane reservoir buffering membrane tension. *Biophys J* 77: 1992–2002, 1999.

Sheetz MP and Singer SJ. Biological membranes as bilayer couples. III. Compensatory shape changes induced in membranes. *J Cell Biol* 70: 193–203, 1976.

Shehata WE, Brownell WE, and Dieler R. Effects of salicylate on shape, electromotility and membrane characteristics of isolated outer hair cells from guinea pig cochlea. *Acta Otolaryngol* (*Stockh*) 111: 707–718, 1991.

Song Y and Baker NA. Effect of salicylate on lipid bilayer mechanics and electrostatics. In: *Abstracts of the Biophysical Society 49th Annual Meeting*. Long Beach, CA, February 12–16, 2005.

Waugh RE. Surface viscosity measurements from large bilayer vesicle tether formation: II. Experiments. *Biophys J* 38: 29–37, 1982.

Waugh RE, Song J, Svetina S, and Zeks B. Local and nonlocal curvature elasticity in bilayer membranes by tether formation from lecithin vesicles. *Biophys J* 61: 974–982, 1992.

Zhang P-C, Keleshian AM, and Sachs F. Voltage-induced membrane movement. *Nature* 413: 428–431, 2001.

Zheng J, Shen W, He DZ, Long KB, Madison LD, and Dallos P. Prestin is the motor protein of cochlear outer hair cells. *Nature* 405: 149–155, 2000.